BIO Web of Conferences **8**, 02006 (2017) DOI: 10.1051/bioconf/20170802006
ICMSB2016

The pairwise phase consistency in cortical network and its relationship with neuronal activation

Daming Wang and Yaoru Sun[a]

Department of Computer Science and Technology, Tongji University, Shanghai, China

Abstract. Gamma-band neuronal oscillation and synchronization with the range of 30-90 Hz are ubiquitous phenomenon across numerous brain areas and various species, and correlated with plenty of cognitive functions. The phase of the oscillation, as one aspect of CTC (Communication through Coherence) hypothesis, underlies various functions for feature coding, memory processing and behaviour performing. The PPC (Pairwise Phase Consistency), an improved coherence measure, statistically quantifies the strength of phase synchronization. In order to evaluate the PPC and its relationships with input stimulus, neuronal activation and firing rate, a simplified spiking neuronal network is constructed to simulate orientation columns in primary visual cortex. If the input orientation stimulus is preferred for a certain orientation column, neurons within this corresponding column will obtain higher firing rate and stronger neuronal activation, which consequently engender higher PPC values, with higher PPC corresponding to higher firing rate. In addition, we investigate the PPC in time resolved analysis with a sliding window.

1 Introduction

Neuronal gamma-band oscillation and synchronization (30–100 Hz) have been observed in several cortical and subcortical areas [1-4] and numerous species [1, 5, 6], and suggested to be associated with a variety of cognitive functions, including signals routing [7-9], feature integration [10, 11], selective attention [12, 13], memory [14, 15] and so on. The properties of gamma band oscillation and its role for cognitive functions are extensively investigated [16-18]. A hypothesis, referred to as CTC (Communication through Coherence), often manifests itself as a plausible mechanism for neuronal oscillation [8, 19].

The CTC hypothesis concerns two aspects for two signals, if their amplitudes correlate (power correlation) or if their peaks and valleys align (phase coherence) [20]. With regard to amplitude aspect, increasing the amplitude of the neuronal activity can implement attention selection to a certain sensory stimulus [21]. Besides, switching one of several convergent pathways from asynchronous to oscillatory state can accurately establish signal routing, because the spatial pattern of amplitude of firing rate can reproduce the spatial pattern of firing rates of neuronal population [22]. As for phase aspect, the oscillatory phase, describing the temporal relationship relative to the background

[a] Corresponding author: yaoru@tongji.edu.cn
This work was supported by the National Natural Science Foundation of China (61173116).

oscillation, is a vital oscillatory parameter and proposed to underlie information processing and transferring in brain cortex [23].

The phase of oscillation is indicated to support multiple cognitive functions, for instance feature coding [24, 25]. The phenomenon of theta-phase precession occurs in the hippocampus and the spatial information can be encoded by theta phase. when the animal moves across the place field of a particular neuron, the phase gradually advances towards the peak of the theta cycle [26]. The gamma cycle hypothesis proposes that the gamma cycle is determined by synchronized inhibitory interneurons, and the excitatory input to a pyramidal neuron can be transformed into a temporal code [27]. The physiological experiment in visual cortex of awaken monkey suggests that the phase can be coded systematically as a function of neuronal activation strength in the gamma cycle [28]. Hippocampal theta has also been proposed to implement information encoding and retrieving in different phases of the theta cycle [4, 15, 23]. The oscillatory phase for other cognitive functions is elucidated in information integration [10, 29], phase-dependent coding of memorized objects [30] and letter recognition [31].

Several computational simulations and theoretical analyses also confirm the general functions of oscillatory phase. The phase of oscillation carries information about stimulus identity and can be shifted with stimulus features, with spike phase coding for stimulus strength [32]. The interaction strength between two neuronal groups can also be established by their relative phase [5, 16, 33].

Two aspects correlated with oscillatory phase are taken into account: the phase of oscillation, representing input stimulus or neuronal activation, and the phase synchronization, serving as an instance of CTC approach for signal routing, information communication and selective attention. The spike-LFP phase, a kind of phase representation, relates spike activity to its background LFP (Local field potential) oscillation [34].

With respect to phase synchronization, PLV (Phase Locking Value) [35], general coherence [5] and PPC (Pairwise Phase Consistency) [34, 36] are three major measures, each of which can quantify phase consistency or the strength of rhythmic synchronization. However, both PLV and general coherence approaches are strongly influenced by the variable and uncontrollable sample size, such as different spike and trial numbers. In order to overcome this bias influence, the PPC measure is introduced, which executes the computation of vector dot product instead of the operation of vector addition across pairs of oscillatory phases [36]. Unfortunately, there still exists further obstacles for PPC approach and a revised version of point-field PPC $\hat{P}_1$, with respect to spike-LFP phase, is proposed. The point-field PPC $\hat{P}_1$ measure only implements dot product computations across different trials in order to eliminate the phase dependence within the same trial, which is induced by non-Poisson history effects, such as refractoriness and bursting [34].

In this experiment, we construct a spiking neuronal network to simulate activities of orientation columns in primary visual cortex, which is inspired by the physiological experiment in visual cortex of awaken monkeys [28]. The properties of PPC and its relationships with input stimulus, orientation preference, firing rate and neuronal activation are extensively investigated and thoroughly demonstrated. The PPC, statistically quantifying the consistency of oscillatory phases, shows significant values all within the frequency of gamma-band. When the input orientation is similar to or as same as the preferred orientation of a certain column, higher firing rate and stronger neuronal activation will be brought about for this corresponding column, which consequently leads to higher PPC values.

2 Methods

2.1 Neuronal model

A leaky integrate-and-fire neuronal model is adopted in this paper, which evolves according to the following equation [37]:

$$C_m \frac{\mathrm{d}V}{\mathrm{d}t} = -g_L(V - V_{rest}) + I_{AMPA} + I_{GABA} + I_{bg} \quad (1)$$

, where C_m is a membrane capacitance, g_L a membrane leak conductance, and I_{bg} a constant tonic background current. When the membrane potential V surpasses the threshold potential of V_{thres}, an action potential is engendered, then the membrane potential V is reset to the resting potential V_{rest}, and it remains clamped for a refractory period of T_{ref}. The excitatory (AMPA) and inhibitory (GABA) synaptic currents I_{AMPA} and I_{GABA} obey (2) and (3)

$$I_{AMPA} = g_{AMPA}(V_E - V) \quad (2)$$

$$I_{GABA} = g_{GABA}(V_I - V) \quad (3)$$

, where V_E and V_I are excitatory and inhibitory reversal potential respectively. The dynamics of the excitatory and inhibitory conductance g_{AMPA} and g_{GABA} comply with the equations as below:

$$\frac{\mathrm{d}g_{AMPA}}{\mathrm{d}t} = -\frac{g_{AMPA}}{\tau_{AMPA}} \quad (4)$$

$$\frac{\mathrm{d}g_{GABA}}{\mathrm{d}t} = -\frac{g_{GABA}}{\tau_{GABA}} \quad (5)$$

, where τ_{AMPA} and τ_{GABA} are excitatory and inhibitory synaptic decay time, and the default values of all parameters can be referred to the Table 1 in the following section.

2.2 Network Architecture

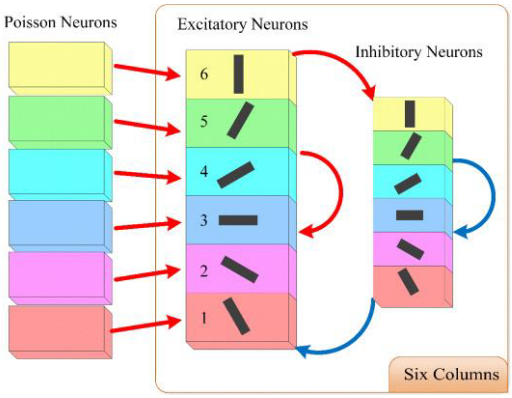

Figure 1. Network architecture

The architecture of neuronal network is elucidated in Figure 1, the left part of which is six groups of Poisson neurons, providing external spike inputs, and the right is six columns, simulating orientation columns in the primary visual cortex. There are 1200 Poisson neurons, 200 for each Poisson group, and totally 1200 excitatory neurons and 300 inhibitory neurons in the six orientation columns. Each of the six orientation columns, decorated with same color, is comprised of 200 excitatory and 50 inhibitory neurons. The ratio of excitatory neurons is 80%, which is in accordance with the experimental evidence [38]. The red and blue arrows represent excitatory and inhibitory synaptic connections respectively, with the parameter $\varepsilon = 0.2$ as their connection probability.

Owing to orientation selectivity and tuning curve of firing rate with regard to stimulus orientation in visual cortex [39], both excitatory and inhibitory neurons in each column are specified with a preferred orientation, with $-\frac{\pi}{3} + \frac{\pi}{6}i$ for the ith column. Therefore the vector of preferred orientation

for six columns is $\left\{-\frac{\pi}{3},\ -\frac{\pi}{6},\ 0,\ \frac{\pi}{6},\ \frac{\pi}{3},\ \frac{\pi}{2}\right\}$. Besides, the same orientation preference is also assigned to the neurons of Poisson groups as their corresponding orientation columns, and Poisson rate is determined according to (6):

$$R_{input} = \left[\cos\left(2\left(\theta_{pref} - \theta_{stim}\right)\right) + 1\right] F_{max} \tag{6}$$

, where θ_{pref} and θ_{stim} are the preferred orientation of Poisson neuron and the stimulus orientation respectively, F_{max} the maximal Poisson firing rate.

There are forward connections from Poisson groups to their corresponding columns, the weights (W_f) of which are all the same and constant. Whereas the connection weights within six orientation columns depend on the difference of preferred orientation between presynaptic and postsynaptic neurons.

$$W_{ij} = \mathrm{W}\exp\left(\beta\left[\cos\left(2\left(\theta_{pre} - \theta_{post}\right)\right) - 1\right]\right) \tag{7}$$

, where θ_{pre} and θ_{post} denote the preferred orientations for presynaptic and postsynaptic neurons respectively.

The LFP data is simulated as the sum of the absolute values of constant background current, excitatory and inhibitory synaptic currents from all excitatory neurons within a nearby neuronal group [40].

$$\mathrm{LFP} = \mathrm{R}\left(\sum_{i=1}^{n}\left(|I_{AMPA}| + |I_{GABA}| + \left|I_{bg}\right|\right)\right) \tag{8}$$

, where the parameter R represents the impedance of electrodes [41].

2.3 Experiment simulating

In the middle of each orientation column, we continuously select 10 excitatory neurons and record their spike activities (action potentials) and synaptic currents, which bring about one LFP channel data. In consequence, there are totally 6 LFP and 60 neuron channels to simulate 6 recording sites by means of intracranial electrodes.

We implement 15 trials altogether for this experiment. For each trial, there is a pre-stimulus baseline period of 500 ms, during which only a tonic background current I_{bg} and low Poisson spike inputs with a rate of F_{bg} are supplied, which simulates the spontaneous activity in visual cortex. Then a constant orientation of 30 degrees is presented for a duration of 1500 ms, in order to mimic the drifting gratings. The input orientation is as same as the preferred orientation of the fourth column, which renders neurons within this column have higher firing rate, stronger neuronal activation and higher phase consistency.

For each spike from a certain neuron channel, six LFP segments except the one within the same column are cut out, all with the spike time as their segments center. Through Discrete Fourier Transform with a Hanning window, all LFP segments are decomposed into spike-triggered LFP spectrum by (9)

$$\bar{X}_i(f) = \frac{1}{5}\sum_{j=1}^{5}\frac{X_i^j(f)}{\left|X_i^j(f)\right|} \tag{9}$$

, where $X_i^j(f)$ denotes the spike-triggered LFP spectrum from the jth LFP channel and ith spike of a certain neuron. Then the spike-LFP phase can be easily obtained through (10) [28].

$$\Theta_i = \mathrm{angle}\left(\bar{X}_i(f)\right) \tag{10}$$

, the angle function obtains the phase angle of the input spectrum. The term $\boldsymbol{U}_{k,m}$ is a vector representation of spike-LFP phase Θ_i. Then we can determine point-field PPC $\hat{P}_1$ with the help of the following equation [34]:

$$\hat{P}_1 = \frac{\sum_{m\in M}\sum_{l\in L}\sum_{k=1}^{N_m}\sum_{j=1}^{N_l}(\boldsymbol{U}_{k,m}\cdot\boldsymbol{U}_{j,l})}{\sum_{m\in M}\sum_{l\in L}(N_m N_l)} \tag{11}$$

, where M and L represent the trial number, N_m and N_l denote the spike number for trial m and trial l.

Finally, we demonstrate time resolved analyses with a sliding window, and the window length and time step are 75 ms and 10 ms respectively. All the neuronal model simulation and network construction are conducted on the basis of an open source Python package of Brian simulator, with a time step 0.1 ms. Then the following spectral analyses are implemented based on a MATLAB toolbox FieldTrip. In addition, the parameters encountered in previous sections are set according to the Table 1:

Table 1. Parameter Settings.

Parameter	Value	Parameter	Value	Parameter	Value	Parameter	Value
C_m	250 pF	g_L	10 nS	V_{rest}	-65 mV	V_{thres}	-45 mV
I_{bg}	300 pA	V_E	0 mV	V_I	-75 mV	τ_{AMPA}	5 ms
τ_{GABA}	10 ms	T_{ref}	5 ms	F_{max}	40 Hz	ε	0.2
β	2	W_f	0.05	R	1.0 MΩ	F_{bg}	3 Hz

3 Results

3.1 Neuronal activities

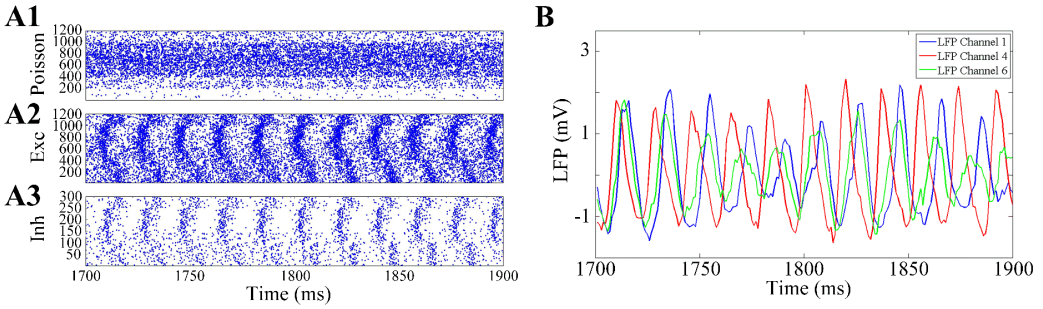

Figure 2. Spike raster and LFP oscillation.
(A) Spike raster of 200 ms period for (A1) Poisson neurons, (A2) excitatory neurons, (A3) inhibitory neurons. (B) Three time sequences of LFP oscillations for the first, fourth and sixth orientation columns.

As demonstrated in Figure 2A, there are three spike raster plots of 200 ms period, representing for Poisson, excitatory and inhibitory neurons respectively. Each interval between index numbers in the vertical coordinate corresponds to one orientation column. Owing to the Poisson rate vector of {3 Hz, 23 Hz, 63 Hz, 83 Hz, 63 Hz, 23 Hz} for six Poisson groups, determined by the differences between preferred orientation of Poisson groups and stimulus orientation, the spike raster of Poisson neurons from the fourth column is densest and gradually declines upwards and downwards to other columns

(Figure 2A1). According to experimental evidences [12], individual neurons fire irregularly, whereas population neurons fluctuate approximately at a certain frequency, giving rise to appropriate oscillation and synchronization. It has been observed that there are strong oscillations in both pyramidal and inhibitory neurons, both around the frequency of 55 Hz (Figures 2A2 and 2A3). If not mentioned otherwise, the subsequent spectral analyses, i.e. PPC computing, are all restricted to this frequency.

We record three LFP oscillation traces from the first, fourth and sixth orientation columns, the peaks of which are entirely different, with the channel four, six and one as a peak time sequence (Figure 2B). Because spikes are more likely to discharge in the trough of the LFP oscillation [41], neurons in the fourth column will fire early with greater likelihood, and then the sixth and first columns, which accounts for the generation of different oscillatory phases and distinct PPC values.

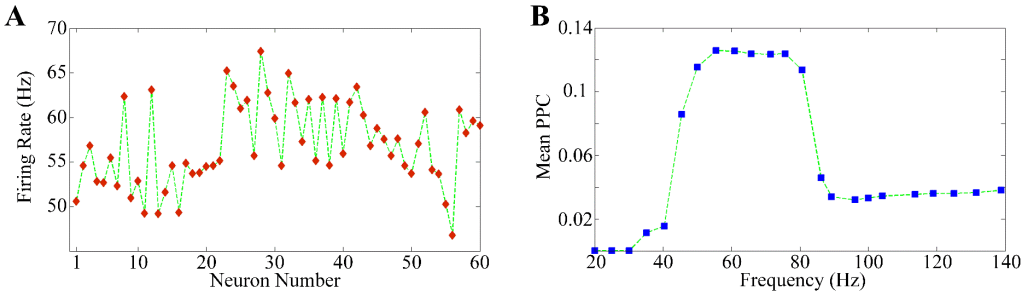

Figure 3. Neuronal firing rate and mean PPC.
(A) Neuronal firing rates of 60 neurons across 15 trials. (B) Mean PPC averaged across 60 neuron channels as a function of frequency

The neuronal firing rates of all 60 neurons across 15 trials are precisely computed and exhibited in Figure 3A. Though to a certain degree do the firing rates of all neurons fluctuate, there are higher firing rates for the third, fourth and fifth columns, and lower firing rates for other columns, because of different orientation preference and the tuning curves of Poisson rates.

Through the measure of point-field PPC $\hat{P}_1$, we calculate PPC for each neuron and then average them to obtain the mean PPC as a function of frequency (Figure 3B). The mean PPC value, with a peak at 55 Hz, demonstrates significant phase consistency all within the frequency of gamma range, which is consistent with the monkey physiological experiment [28].

3.2 Pairwise phase consistency

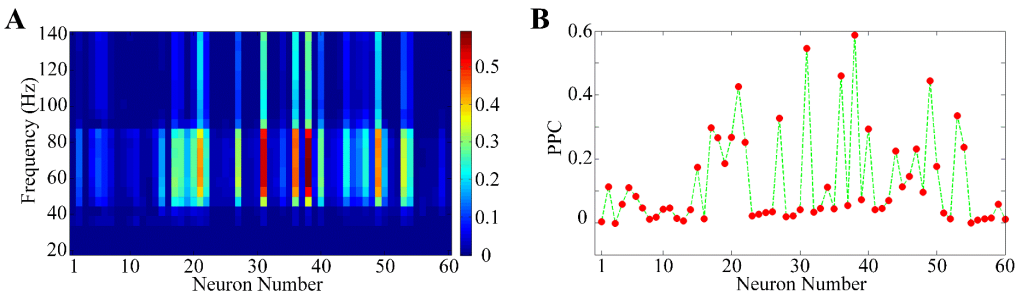

Figure 4. PPC of 60 neurons.
(A) PPC of 60 neurons for the frequency range of 20-140 Hz. (B) PPC of 60 neurons at 55 Hz

The PPC values of all 60 neurons, with the frequency range of 20-140 Hz, are thoroughly elucidated in Figure 4A, which are derived by means of point-field PPC $\hat{P}_1$ approach. The significant phase consistency values of all neurons are all within the frequency of gamma-band. Furthermore, the PPC

values for the fourth orientation column are the most powerful and gradually decrease towards left and right to other columns. We select the PPC at the frequency of 55 Hz, the same frequency of LFP oscillation, and illustrate it as a function of neuron number (Figure 4B).

The input orientation of 30 degrees is the same as the preferred orientation of the fourth column, which gives rise to stronger Poisson inputs, higher firing rates and neuronal activation. Thus the spikes are more likely to be concentrated on a certain part of LFP oscillations and therefore lower phase dispersions are engendered. Consequently, the PPC measure, quantifying the consistency of oscillatory phases, obtains higher values in the fourth column, and declines gradually to its nearby columns.

3.3 Time resolved analysis

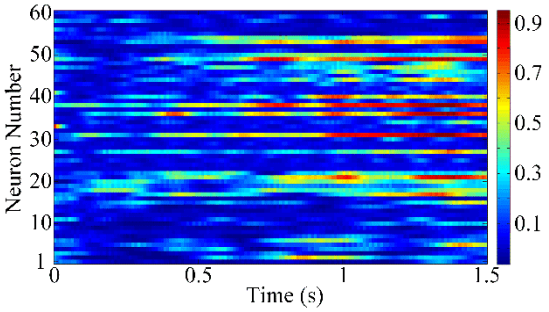

Figure 5. Time resolved analysis of PPC for 60 neurons.

With a sliding window, we analyze the PPC values of all 60 neurons in a time resolved way (Figure 5). The PPC manifests higher values for neurons from the fourth orientation column, and then decreases gradually upwards and downwards to other columns. Though neurons within the same orientation column receive the same Poisson input and obtain similar neuronal activation, the PPC of which are not always the same, but slightly different across different neurons for the same column. Additionally, the PPC for the beginning period is considerably small and comparatively similar across all 60 neurons because of the transient stimulus onset effect.

4 Conclusions

In order to investigate the oscillatory phase, PPC and their relationships with input orientation, firing rate and neuronal activation, we construct a spiking neuronal network according to the physiological experiment of awaken monkeys [28]. Six Poisson groups, with different Poisson rates, provide external spike inputs and six columns, with distinct orientation preference, simulate orientation columns in primary visual cortex. Then we conduct data recording and spectral analyses, which include spike-LFP phase calculation [28] and point-field PPC $\hat{P}_1$ computation [34]. The most powerful PPC values of neurons are all within the gamma-band frequency, which is consistent with physiological experiments [28]. If the preferred orientation of one column is close or equivalent to the input orientation stimulus, the neurons within this column will obtain higher firing rate and stronger activation, thereby giving rise to stronger synchronization and higher PPC values. However, the PPC will degrade if the input orientation is far from the preferred orientation of a certain column. Furthermore, we adopt the leaky integrate-and-fire neuronal model because of its biological plausibility and computational efficiency, however other models such as Hodgkin–Huxley model and SRM model are feasible.

References

1. C. M. Gray, P. Konig, A. K. Engel, W. Singer. *NATURE* **338**, 334-337 (1989).
2. J. M. Schoffelen, R. Oostenveld, P. Fries. *SCIENCE* **308**, 111-113 (2005).
3. T. Spellman, M. Rigotti, S. E. Ahmari, S. Fusi, J. A. Gogos, J. A. Gordon. *NATURE* **522**, 309 (2015).
4. K. M. Igarashi, L. Lu, L. L. Colgin, M. Moser, E. I. Moser. *NATURE* **510**, 143 (2014).
5. T. Womelsdorf, J. Schoffelen, R. Oostenveld, W. Singer, R. Desimone, A. K. Engel, P. Fries. *SCIENCE* **316**, 1609-1612 (2007).
6. R. T. Canolty, E. Edwards, S. S. Dalal, M. Soltani, S. S. Nagarajan, H. E. Kirsch, M. S. Berger, N. M. Barbaro, R. T. Knight. *SCIENCE* **313**, 1626-1628 (2006).
7. E. Salinas, T. J. Sejnowski. *NAT REV NEUROSCI* **2**, 539-550 (2001).
8. P. Fries. *TRENDS COGN SCI* **9**, 474-480 (2005).
9. T. Akam, D. M. Kullmann. *NAT REV NEUROSCI* **15**, 111-122 (2014).
10. W. Singer, C. M. Gray. *ANNU REV NEUROSCI* **18**, 555-586 (1995).
11. N. Brunet, C. A. Bosman, M. Roberts, R. Oostenveld, T. Womelsdorf, P. De Weerd, P. Fries. *CEREB CORTEX* **25**, 918-926 (2015).
12. P. Fries, J. H. Reynolds, A. E. Rorie, R. Desimone. *SCIENCE* **291**, 1560-1563 (2001).
13. D. Baldauf, R. Desimone. *SCIENCE* **344**, 424-427 (2014).
14. B. Pesaran, J. S. Pezaris, M. Sahani, P. P. Mitra, R. A. Andersen. *NAT NEUROSCI* **5**, 805-811 (2002).
15. J. Fell, N. Axmacher. *NAT REV NEUROSCI* **12**, 105-1500 (2011).
16. P. Fries. *ANNU REV NEUROSCI* **32**, 209-224 (2009).
17. G. Buzsaki, X. J. Wang. *ANNU REV NEUROSCI* **35**, 203-225 (2012).
18. C. A. Bosman, C. S. Lansink, C. M. A. Pennartz. *EUR J NEUROSCI* **39**, 1982-1999 (2014).
19. P. Fries. *NEURON* **88**, 220-235 (2015).
20. A. Z. Harris, J. A. Gordon. *ANNU REV NEUROSCI* **38**, 171-194 (2015).
21. M. Zeitler, P. Fries, S. Gielen. *J COMPUT NEUROSCI* **25**, 89-107 (2008).
22. T. Akam, D. M. Kullmann. *NEURON* **67**, 308-320 (2010).
23. M. A. Wilson, C. Varela, M. Remondes. *CURR OPIN NEUROBIOL* **31**, 250-253 (2015).
24. M. A. Montemurro, M. J. Rasch, Y. Murayama, N. K. Logothetis, S. Panzeri. *CURR BIOL* **18**, 375-380 (2008).
25. C. Kayser, M. A. Montemurro, N. K. Logothetis, S. Panzeri. *NEURON* **61**, 597-608 (2009).
26. J. O'Keefe, M. L. Recce. *HIPPOCAMPUS* **3**, 317-330 (1993).
27. P. Fries, D. Nikolic, W. Singer. *TRENDS NEUROSCI* **30**, 309-316 (2007).
28. M. Vinck, B. Lima, T. Womelsdorf, R. Oostenveld, W. Singer, S. Neuenschwander, P. Fries. *J NEUROSCI* **30**, 1250-1257 (2010).
29. T. Womelsdorf, P. Fries. *J PHYSIOL-PARIS* **100**, 182-193 (2006).
30. M. Siegel, M. R. Warden, E. K. Miller. *P NATL ACAD SCI USA* **106**, 21341-21346 (2009).
31. R. Polania, M. A. Nitsche, C. Korman, G. Batsikadze, W. Paulus. *CURR BIOL* **22**, 1314-1318 (2012).
32. P. H. Tiesinga, T. J. Sejnowski. *FRONT HUM NEUROSCI* **4** (2010).
33. A. Buehlmann, G. Deco. *PLOS COMPUT BIOL* **6**, e1000934 (2010).
34. M. Vinck, F. P. Battaglia, T. Womelsdorf, C. Pennartz. *J COMPUT NEUROSCI* **33**, 53-75 (2012).
35. J. P. Lachaux, E. Rodriguez, J. Martinerie, F. J. Varela. *HUM BRAIN MAPP* **8**, 194-208 (1999).
36. M. Vinck, M. van Wingerden, T. Womelsdorf, P. Fries, C. M. A. Pennartz. *NEUROIMAGE* **51**, 112-122 (2010).
37. T. P. Vogels, H. Sprekeler, F. Zenke, C. Clopath, W. Gerstner. *SCIENCE* **334**, 1569-1573 (2011).
38. H. Hu, J. Gan, P. Jonas. *SCIENCE* **345**, 529 (2014).
39. D. Ferster, K. D. Miller. *ANNU REV NEUROSCI* **23**, 441-471 (2000).
40. A. Mazzoni, S. Panzeri, N. K. Logothetis, N. Brunel. *PLOS COMPUT BIOL* **4**, e1000239 (2008).
41. A. Barardi, B. Sancristobal, J. Garcia-Ojalvo. *PLOS COMPUT BIOL* **10**, e1003723 (2014).